Int. J. Heat Mass Transfer. Vol. 35, No. 5, pp. 1209–1228, 1992
Printed in Great Britain

0017–9310/92 $5.00+0.00

Mixed convection analysis in large baffled rectangular chambers with internal heat sources

K. L. YERKES† and A. FAGHRI
Wright State University, Department of Mechanical and Materials Engineering, Dayton, OH 45435, U.S.A.

(*Received* 15 *October* 1990 *and in final form* 30 *April* 1991)

Abstract—An investigation to determine the effects of mixed convection on the flow structure of large baffled chambers with internal heat sources has been completed. Baffles and internal heat sources are placed symmetrically about the vertical axis while maintaining a constant and uniform inlet velocity, inlet temperature, and wall temperature. Time-dependent experimental and two-dimensional numerical results are compared at various chamber locations to demonstrate the transition of the flow structure through a sequence of bifurcations with increasing internal heat source temperatures.

INTRODUCTION

LARGE baffled rectangular chambers with low inlet velocities have traditionally been used to study a variety of chemical atmospheres generated for health effects and biological studies, chemical reaction and chemical species formation studies, and aerosol characterization studies. Generally, they have a cross-sectional diameter greater than 0.5 m with an inlet velocity set to maintain 10–15 chamber volume changes per hour. The inlet and exhaust may be mounted vertically or horizontally with an array of internal baffles included for atmosphere dispersion purposes. Additional capabilities include cage units for housing laboratory animals for a variety of biological research applications.

There have been many investigations concerning the Rayleigh–Bénard flow in confined and partially open enclosures with and without baffles or dividers and internal or wall heat sources [1–9]. Such investigations have made use of both experimental and numerical results for information with regard to the temperature profile and flow structure in various closed cavity geometries with differing magnitude of Grashof, Prandtl, and Rayleigh numbers.

Yang [10] discussed the buoyant enclosure problem as a dissipative dynamic system whose flow structure development is one of a series of bifurcations brought about by the driving parameters of Rayleigh number, Prandtl number, and enclosure geometry. Development of a flow structure from one that is steady state, periodic in time, aperiodic, and finally chaotic are examples of specific bifurcations that may be expected with variation in Rayleigh number, Prandtl number, and altered geometry. Yang [10] further discussed the use of an attractor, a concept used in nonlinear dynamics, to describe the temporal asymptotic behavior of a trajectory in the phase space corresponding to a specific bifurcation.

Initial investigations of these chambers incorporated flow visualization techniques using smoke and dyes to optimize the chamber geometry so that well-dispersed atmospheres could be obtained [11, 12]. Quantitative studies to determine the mean residence time of a chamber, the rate of dispersion within a chamber of a tracer gas, and the distribution within a chamber using vapors, droplets, and solid particles have also been performed [13–16]. Most recently, Yerkes and Faghri [17] investigated the mixed convection in large baffled rectangular chambers and the characteristic flow structure development for 'aided' and 'opposed' buoyant forces. Development of the chamber flow structure was found to be predominantly buoyant in nature and sensitive to small variations in the temperature difference between the inlet and wall, varying from steady state to asymmetric oscillatory behavior.

These investigations have not addressed the effects of mixed convection with internal biological heat sources on the transport phenomenon of heat and mass transfer within these chambers. Information into the diffusion and convection of mass, enthalpy, and momentum within these chambers with the biological heat sources are of interest to better understand their operation and provide a basis for improvement, modification and future development. Therefore, the objective of this study was to develop a numerical algorithm and experimental method by which the frequencies at which specific bifurcations occur can be predicted. The numerical algorithm was based on the conservation laws of mass, momentum, and energy, and the experimental model simulated the larger, full-size chamber.

A typical chamber that may be used for the purposes described consists of a conical inlet intended to

† Presently with Wright Research and Development Center, Wright-Patterson AFB, Ohio, U.S.A.

NOMENCLATURE

B_z	body force vector in z-direction
C_p	specific heat [J kg^{-1} K^{-1}]
D	depth of chamber [m]
D_h	hydraulic diameter, $2LD/(L+D)$
g	acceleration due to gravity [m s^{-2}]
Gr	Grashof number, $g\beta D_h^3 \delta T/\nu^2$
H	height of chamber [m]
h	hydrostatic height [m]
k	thermal conductivity [W m^{-1} K^{-1}]
L	width of chamber [m]
p^+	pressure due to motion and hydrostatic pressure, $p^* - \rho g h$ [N m^{-2}]
p^*	pressure due to motion (static pressure) [N m^{-2}]
Pr	Prandtl number, $\mu C_p/k$
Ra	Rayleigh number, $GrPr$
Re	inlet Reynolds number, $D_h W_{IN}/\nu$
T	temperature [K]
T_{IN}	inlet temperature [K]
T_{sw}	side wall temperature [K] (see Fig. 1)
T_w	end wall temperature [K] (see Fig. 1)
t	time [s]
v	y-direction velocity [m s^{-1}]
w	z-direction velocity [m s^{-1}]
W_{IN}	inlet vertical velocity [m s^{-1}]
y	horizontal coordinate [m]
z	vertical coordinate [m].

Greek symbols

β	coefficient of thermal expansion, $-(1/\rho)(\partial\rho/\partial T)$ [K^{-1}]
δT	$(T_{IN} - T_w)$ [K]
ε	fractional change in dependent variable
μ	dynamic viscosity [kg m^{-1} s^{-1}]
ν	kinematic viscosity [m^2 s^{-1}]
ρ	fluid density [kg m^{-3}]
ϕ	dependent variable
ϕ_s	dependent variable at specific sweep or time step.

uniformly distribute the atmosphere of interest across the inlet plane. The exhaust consists of a manifold to achieve uniform flow characteristics across the exhaust plane. Inlet and exhaust flow rates are controlled independently to maintain a slightly negative chamber pressure with respect to the ambient (2.5–5.1 cm H_2O). Biological heat sources may consist of a variety of laboratory animal species and are housed in uniformly spaced cage units located directly over the baffles.

This investigation considers a simplified version of the aforementioned chamber. Of interest is the transient behavior and development of the flow structure due to a temperature gradient between the biological heat sources, inlet temperature and wall temperature. The vertical end wall temperature, T_w, was assumed to be constant and equal to 24°C due to the thin wall construction. The inlet temperature was also assumed to be constant across the inlet plane and equal to 27°C. Biological heat sources were treated as cubes with constant-temperature surfaces held at 32°C and of a size and mass that would be appropriate for a 200–300 g rat in a confined enclosure [18]. It was assumed that physiological control of the body temperature is sufficient to maintain a constant body temperature in the low air velocities within the confines of the chamber.

Typical values of Grashof, Rayleigh and Reynolds numbers were $Gr = 2.02 \times 10^6$, $Ra = 1.42 \times 10^6$ and $Re = 32$ and 235 using the inlet hydraulic diameter, D_h, as the characteristic length. The two-dimensional formulation assumed a chamber depth of 1 m while the experimental model had a depth of 6.67 cm, thereby resulting in different Reynolds numbers due to the differing hydraulic diameters. The difference in temperature was taken to be the maximum difference between the vertical and wall temperature and the biological heat source temperature, $\delta T_{max} = 8.0$°C, with an inlet velocity of 4.1×10^{-3} m s^{-1}. With these values for Grashof, Rayleigh and Reynolds numbers, the development of the flow structure was predominantly buoyant in nature.

ANALYSIS

Two-dimensional numerical solutions of the incompressible time-dependent laminar Navier–Stokes equations were calculated corresponding to the schematic shown in Fig. 1(a). Only the dimensional forms of the governing equations were solved, thereby circumventing the immediate need for scaling considerations of the nondimensional parameters as is typically required for buoyant flow conditions [9]. The Boussinesq approximation was used in the vertical direction to account for buoyancy effects. Using this approximation the vertical body force becomes:

$$B_z = \rho g[1 - \beta(T - T_{IN})]$$

where

$$\beta = \frac{1}{T_{IN}}$$

for an ideal gas. The reference values for all of the gas properties were taken to be those at the inlet plane.

The chamber inlet conc was assumed to provide a uniform velocity distribution across the inlet plane. The exhaust manifold was assumed to provide a velocity distribution corresponding to a constant exhaust

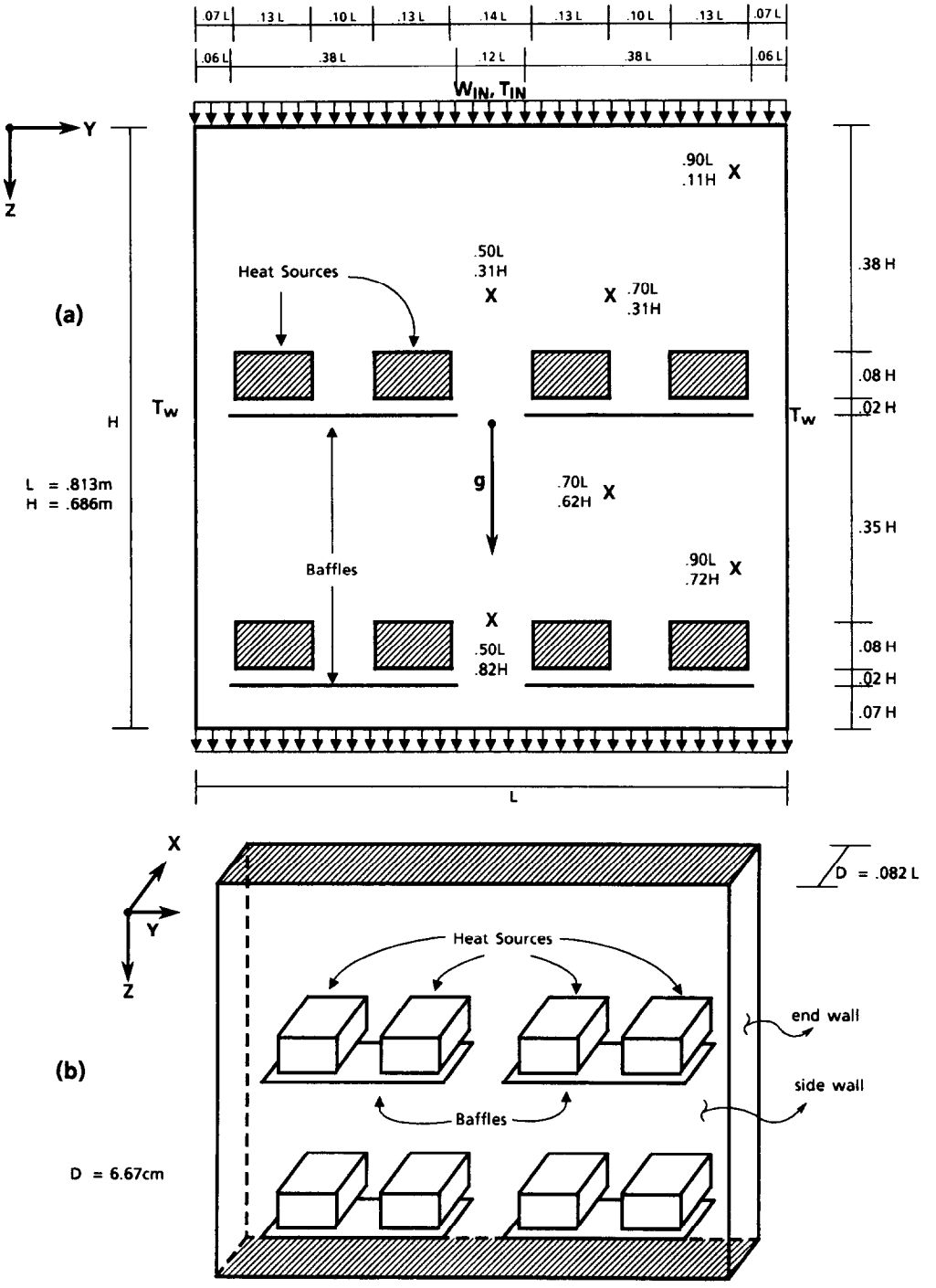

FIG. 1. Chamber geometry specifications. (a) Two-dimensional geometry. (b) Three-dimensional laboratory model geometry.

pressure across the outlet plane. Viscous dissipation and pressure work were assumed to be negligible due to the low buoyancy-induced velocities. With these assumptions, the two-dimensional governing equations become:

Conservation of mass

$$\frac{\partial v}{\partial y}+\frac{\partial w}{\partial z}=0 \tag{1}$$

Conservation of momentum

$$\rho\left(\frac{\partial v}{\partial t}+v\frac{\partial v}{\partial y}+w\frac{\partial v}{\partial z}\right)=-\frac{\partial p^{+}}{\partial y}+\mu\left(\frac{\partial^2 v}{\partial y^2}+\frac{\partial^2 v}{\partial z^2}\right) \tag{2}$$

$$\rho\left(\frac{\partial w}{\partial t}+v\frac{\partial w}{\partial y}+w\frac{\partial w}{\partial z}\right)=-\frac{\partial p^{+}}{\partial z}+\mu\left(\frac{\partial^2 w}{\partial y^2}+\frac{\partial^2 w}{\partial z^2}\right)+\rho g\beta(T-T_{\mathrm{IN}}) \tag{3}$$

Conservation of energy

$$\rho\left(\frac{\partial T}{\partial t}+v\frac{\partial T}{\partial y}+w\frac{\partial T}{\partial z}\right)=\frac{k}{C_p}\left(\frac{\partial^2 T}{\partial y^2}+\frac{\partial^2 T}{\partial z^2}\right). \tag{4}$$

The boundary conditions were as follows:

Inlet: $t \geqslant 0$, $v=0$, $w=W_{\mathrm{IN}}=4.1\times10^{-3}$ m s^{-1}, $T=T_{\mathrm{IN}}=27^{\circ}$C
Vertical end wall: $t \geqslant 0$, $v=0$, $w=0$, $T=T_{\mathrm{w}}=24^{\circ}$C
Baffle: $t \geqslant 0$, $v=0$, $w=0$
Heat sources: $t \geqslant 0$, $T=32^{\circ}$C
Outlet: $t \geqslant 0$, $v=0$, $p^{+}=0$.

The inlet velocity profile, the vertical end wall temperature, and the surfaces of the heat sources were constant. The magnitude of the outlet velocity is such as to satisfy the conservation of mass with a constant reference pressure across the outlet plane. The outlet boundary condition for temperature was considered to be locally parabolic such that the Peclet number is sufficiently large so as to exhibit local one-way behavior in the axial direction.

Two initial (restart) fields were chosen for the initial conditions of the field-dependent variables. The methods for obtaining the restart fields are discussed in the following section.

NUMERICAL SCHEME

The numerical scheme used is a finite-difference iterative method of solution using a control-volume approach as developed by Spalding [19]. The two-dimensional numerical model was formulated using a fully implicit finite-difference scheme of the time-dependent, laminar Navier–Stokes equations. The 'SIMPLEST' [19] method of solution for the momentum equations was used with the hybrid differencing formulation. When a cell Peclet number is within the range -2 to 2, a central-difference scheme is used and when the cell Peclet number is outside this range the upwind differencing scheme is used.

The outlet boundary condition for temperature was considered to be locally parabolic such that the Peclet number is sufficiently large so as to exhibit local one-way behavior in the axial direction [20]. This approach to specifying the outlet boundary condition for a dependent variable is generally accepted as the most available approach for internal flow problems in which the fluid leaves the calculation domain and the dependent variable of interest is unknown.

The baffles were treated as being infinitesimally thick with a no-slip boundary condition by setting the cell wall velocity to zero over the region of the baffle location. The baffle temperature was specified to be that of the local fluid temperature. Heat sources were 'blocked' by setting the cell velocity components within the heat source region to zero and fixing to a constant temperature.

The solution sequence involved solving for the velocity and temperature fields from an assumed pressure field at a specific time step. The pressure field was then subsequently updated using these velocity and temperature fields in the pressure-correction equation such that the conservation of mass was satisfied. This iterative sweep process was then repeated using a slab-by-slab method at each time step until convergence criteria were satisfied. Convergence characteristics at each time step were maintained by reducing the time step where appropriate. Conditions for convergence to a solution, either at a specific time step or to a steady state solution, were based upon a dependent variable, ϕ, varying less than a predetermined change of the magnitude fraction, ε_{ϕ}, between successive sweeps or time steps where

$$|\phi_s-\phi_{s+1}|/\phi \leqslant \varepsilon_{\phi}.$$

The values of ε_{ϕ} were varied and it was required that the magnitude of the dependent variable be greater than the round-off error or truncation error such as would happen when velocities approach zero. Typically, ε_{ϕ} was less than 10^{-3} for five successive sweeps. Intermediate results were monitored to ensure convergence and numerical stability at a specific time step during the course of the solution. These intermediate results were also used to determine convergence toward either a steady state or a steady periodic solution.

Appropriate grid size and spacing and numerical time step were chosen to give acceptable numerical accuracy while still maintaining reasonable computational times. Due to the complexity of the flow structure, the errors as a result of grid size and time step were determined by comparing the shape of the flow structure for similarity with a previous solution at a larger time step or grid size. Also, random locations throughout the chamber were selected and the average error compared between the similar solutions. Reducing the time step by 50% resulted in a less than 3% change in the dependent variable, while decreasing the grid size by 10% resulted in a less than 1% change.

A uniform 100×100 grid was chosen to give good coverage with a time step of 0.010 s.

Initially, the solution was started from a zero velocity and constant temperature field. The time step was gradually reduced once the solution became oscillatory in nature either due to numerical perturbations or naturally occurring oscillations. Two restart fields for velocity, temperature and pressure were then chosen from these solutions and the time dependence behavior was observed over a span of 40 s using the final reduced time step of 0.010 s.

With the development of the relatively complex transient flow structure, both decreasing the grid size and time step would reveal additional frequencies that would otherwise not be observed with a larger grid size and time step. In addition, error propagation with the progression of time would tend to oscillate the solution with numerically-induced low frequency harmonics. Increasing the grid number and reducing the time step would reveal these additional wavelengths and harmonics, and would decrease the time step related propagation errors. Due to the physical size of the problem, however, this would significantly increase the computational time needed to solve the problem.

EXPERIMENTAL APPROACH

An experimental chamber model was fabricated using 1.91 cm thick Plexiglass with interior body dimensions of 0.813 m × 6.67 cm and 0.686 m high, as shown in Figs. 1(b) and 2. Baffles of 1.5 mm thick Plexiglass were inserted across the chamber depth and fixed into the vertical side walls. The vertical end walls were fabricated using a thin aluminum plate combined with a water jacket to maintain a constant wall temperature. A Lauda recycling water bath was used to maintain a constant water temperature in the water jacket (± 0.2°C). Heat sources were simulated using flask heating mantles (Glas-col) located symmetrically approximately 1.4 cm above the baffles and maintained at constant temperature (± 0.5°C). Inlet and exhaust air were passed through a series of laminated porous stainless steel plates with a nominal pore size of 44 μm to maintain a uniform velocity profile. The inlet volumetric flow rate was adjusted and monitored using a Matheson rotameter and corrected to account for the operational pressure drop. The chamber pressure was maintained to that of ambient by adjusting the exhaust flow rate.

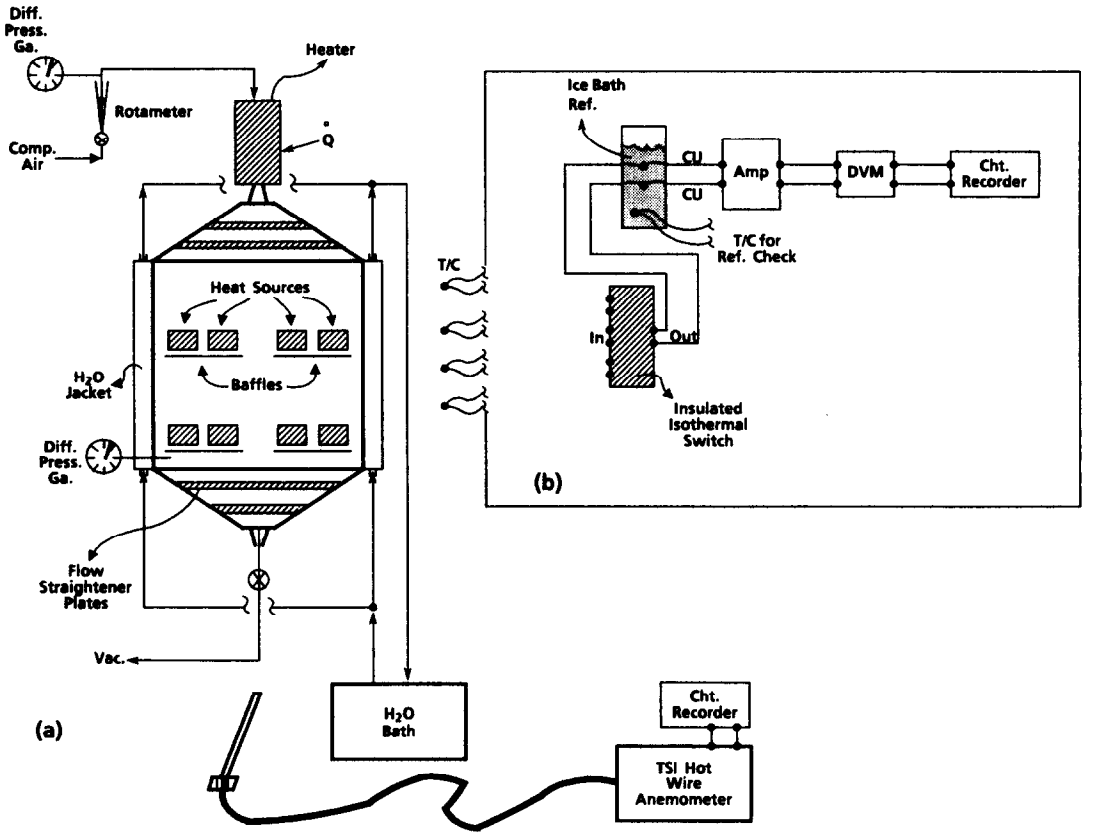

FIG. 2. Experimental apparatus. (a) Laboratory experimental model. (b) Temperature measurement set-up.

Field temperature measurements were made using iron–constantan exposed junction thermocouples individually calibrated to ± 0.1°C. Each thermocouple was immersed in a stirred water bath and calibrated using a standard NBS traceable thermometer (Ever Ready Thermometer Co., New York) which had an uncertainty of ± 0.05°C over the anticipated range of operation of 24–32°C. An insulated isothermal thermocouple switch to minimize stray e.m.f. and a thermocouple amplifier were used in conjunction with a digital voltmeter for a sensitivity greater than the required ± 5.1 μV for ± 0.1°C measurements. Thermocouple voltages over a range of calibration temperatures were obtained and referenced to an ice point consisting of a large reservoir ice bath with an additional reference thermocouple to verify shifts in the reference ice point temperature. The resulting calibration was used to determine the field temperature during the course of experimentation. Periodically, the standard NBS traceable thermometer was also used to verify field temperatures of the experiment.

Thermocouples were chosen and sized to minimize flow disturbances and maximize response time with a sheath diameter of 0.159 cm and a bead diameter ranging from 0.025 to 0.076 cm for a time constant of 1.35–1.73 s. Assuming a maximum time constant of 1.7 s, the frequency response for measuring a 0.017 Hz (1 cycle/60 s) signal would result in a 0.985 attenuation with a $-10°$ phase shift.

Velocity data were obtained using a TSI IFA-100 hot wire anemometer using a platinum film sensor (Model No. 1211-10) with a frequency response of 300 kHz. To effectively use the hot wire anemometer, the magnitude of the buoyant-induced velocity, due to the heating of the sensor, in relation to the velocity to be measured was of interest. Uncertainty errors can be determined depending upon the orientation of the fluid velocity to that of the induced buoyant velocity [21]. This is evident when the stream velocity is either opposed to or in the same direction and of the same order of magnitude as the sensor-induced buoyant velocity. During this experiment, the range of stream velocities encompassed the sensor-induced velocity, limiting the use of the hot wire anemometer from quantitatively evaluating the velocity magnitude to evaluating the frequency behavior of the velocity at various chamber locations.

The laboratory experimental chamber was operated in such a manner so as to observe the development of the transient behavior of both temperature and velocity at six chamber locations (Fig. 1). Initially the chamber was started from a steady state condition without heat sources and with an inlet velocity, W_{IN}, of 4.1×10^{-3} m s^{-1}. The heat sources were gradually brought to 32°C while maintaining the inlet temperature, T_{IN}, and vertical wall temperature, T_w, at 27°C and 24°C, respectively. Temperature and velocity data were obtained at the six chamber locations until the chamber appeared to maintain a steady periodic state in which the magnitude and oscillatory behavior of velocity and temperature remained constant. It was found that simultaneous measurements of velocity and temperature at the same chamber location induced temperature measurement errors due to the hot wire anemometer probe. Therefore, measurements of temperature and velocity were obtained at differing chamber locations.

RESULTS AND DISCUSSION

Experimental data from the laboratory model consisted of time-dependent temperature and hot wire anemometry measurements at various chamber locations about the central plane to determine the transient behavior of temperature and velocity. These experimental data were then compared with results obtained from the transient two-dimensional numerical solutions.

Typical two-dimensional numerical solutions for velocity and temperature at a time $t = t_0$ and $t = t_0 + 30$ s are presented in Figs. 3 and 4, respectively. Figure 5 shows the two-dimensional numerical time-dependent variation of temperature and velocity for six chamber locations [$(0.50L, 0.31H)$, $(0.50L, 0.82H)$, $(0.70L, 0.31H)$, $(0.70L, 0.62H)$, $(0.90L, 0.11H)$, $(0.90L, 0.72H)$]. These numerical solutions were initiated, as discussed in the numerical scheme, from the two arbitrarily chosen initial restart fields spanning a 40 s time frame. The numerical solution phase-space shapes are shown in Fig. 6, plotted as the rate of change of the dependent variable, velocity and temperature vs the dependent variable over time. Experimentally obtained temperature and velocity data with increasing heat source temperature at chamber location $(0.70L, 0.31H)$ are shown in Fig. 7 and at the six chamber locations in Fig. 8. In these figures, 48 s snapshots were taken at 10 min intervals for 120 min to demonstrate the transient behavior of the chamber as the heat source temperature is increased. These experimental data are also compared to the time-dependent velocity obtained from the numerical results, which are also shown in Fig. 8.

Development of the flow structure (Figs. 3 and 4) was found to be time-dependent in nature with the formation of four Bénard cells above the upper baffles and heat sources. Over the course of time, these cells dissipated and reformed, resulting in an oscillating core flow between the two upper baffles. A high velocity wall boundary layer flow was maintained on the vertical end wall, increasing in thickness as the core flow dissipated. Bénard cells also formed between the upper and lower sets of baffles, although the formation of these cells appeared to be influenced by the core flow. There was a reflux of mass between the vertical walls and upper baffles that was also influenced by the oscillating core flow, which in turn influenced the formation of the Bénard cells above the upper baffles and heat sources. This behavior resulted in a marginally stable and oscillatory flow structure.

Two-dimensional numerical results showed that the

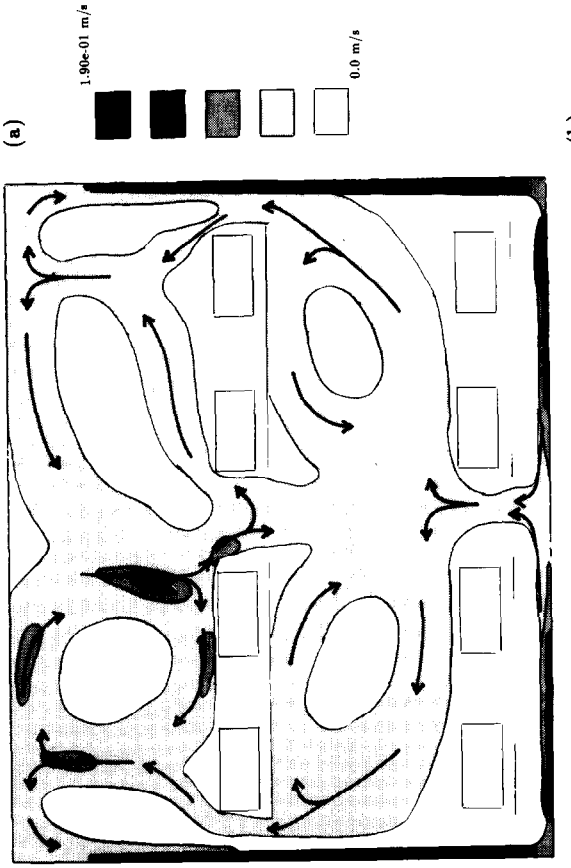

FIG. 3. Two-dimensional numerical results at time $t = t_0$. (a) Chamber velocity direction and magnitude profile. (b) Temperature contour.

FIG. 4. Two-dimensional numerical results at time $t = t_0 + 30$ s. (a) Chamber velocity direction and magnitude profile. (b) Temperature contour.

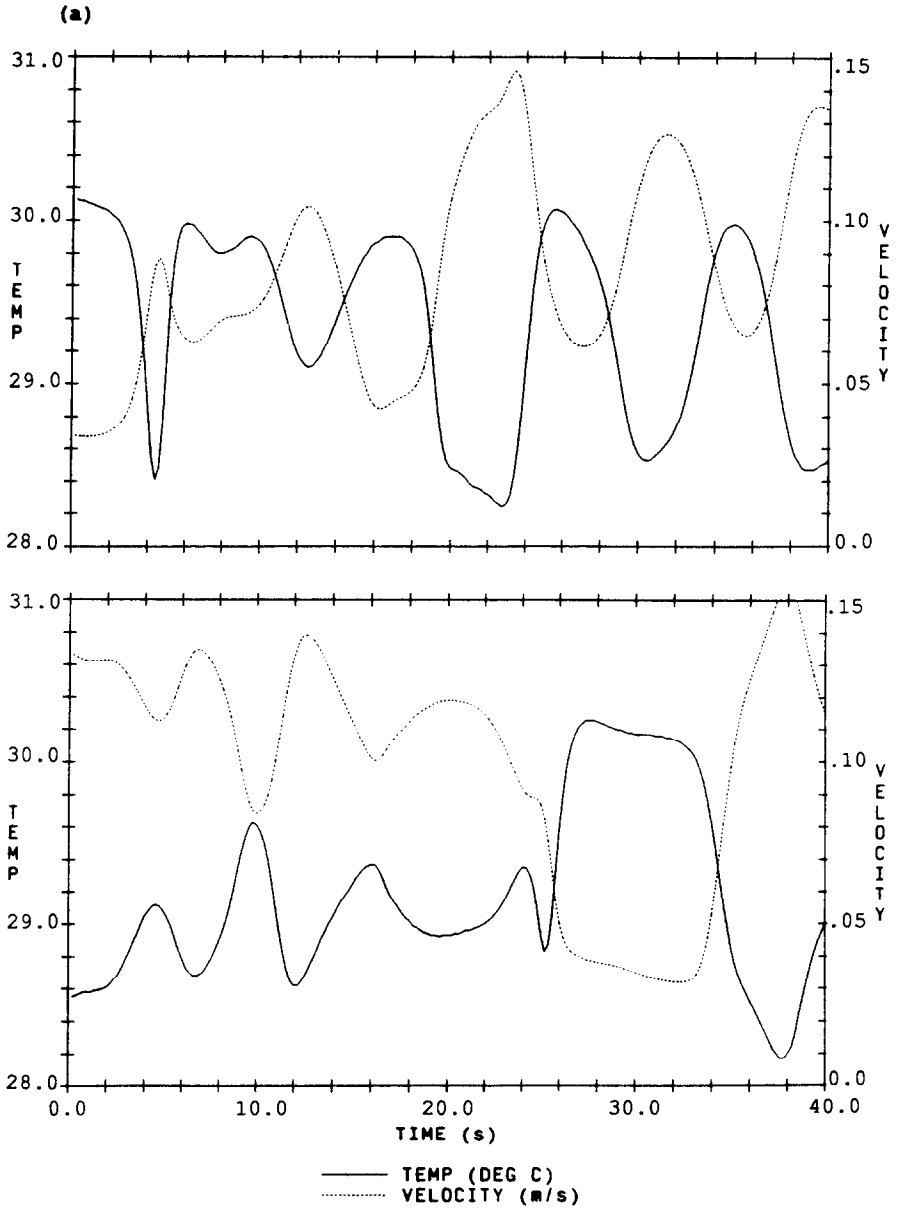

FIG. 5. Two-dimensional numerical time-dependent plots of velocity and temperature. (a) (0.50L, 0.31H). (b) (0.70L, 0.31H). (c) (0.90L, 0.11H). (d) (0.50L, 0.82H). (e) (0.70L, 0.62H). (f) (0.90L, 0.72H).

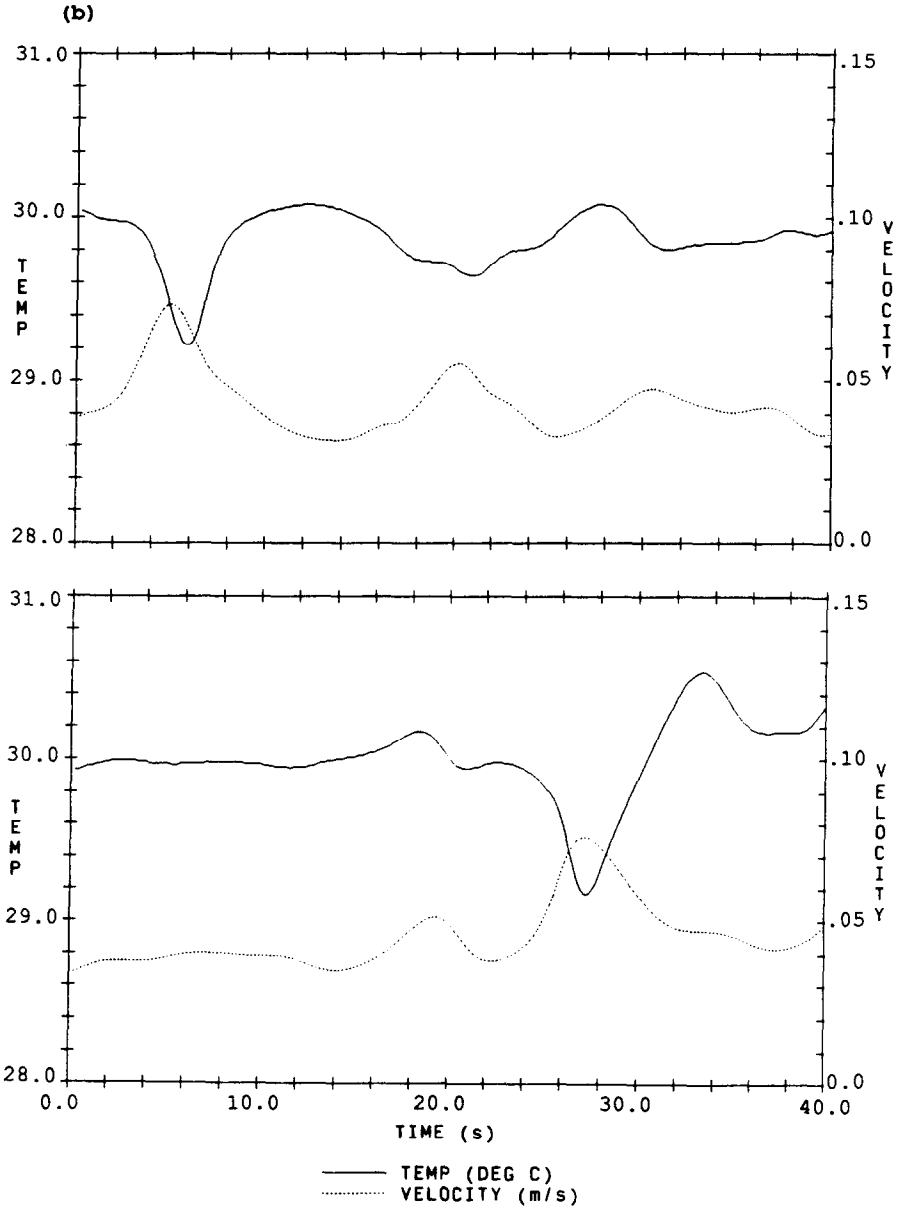

FIG. 5.—*Continued.*

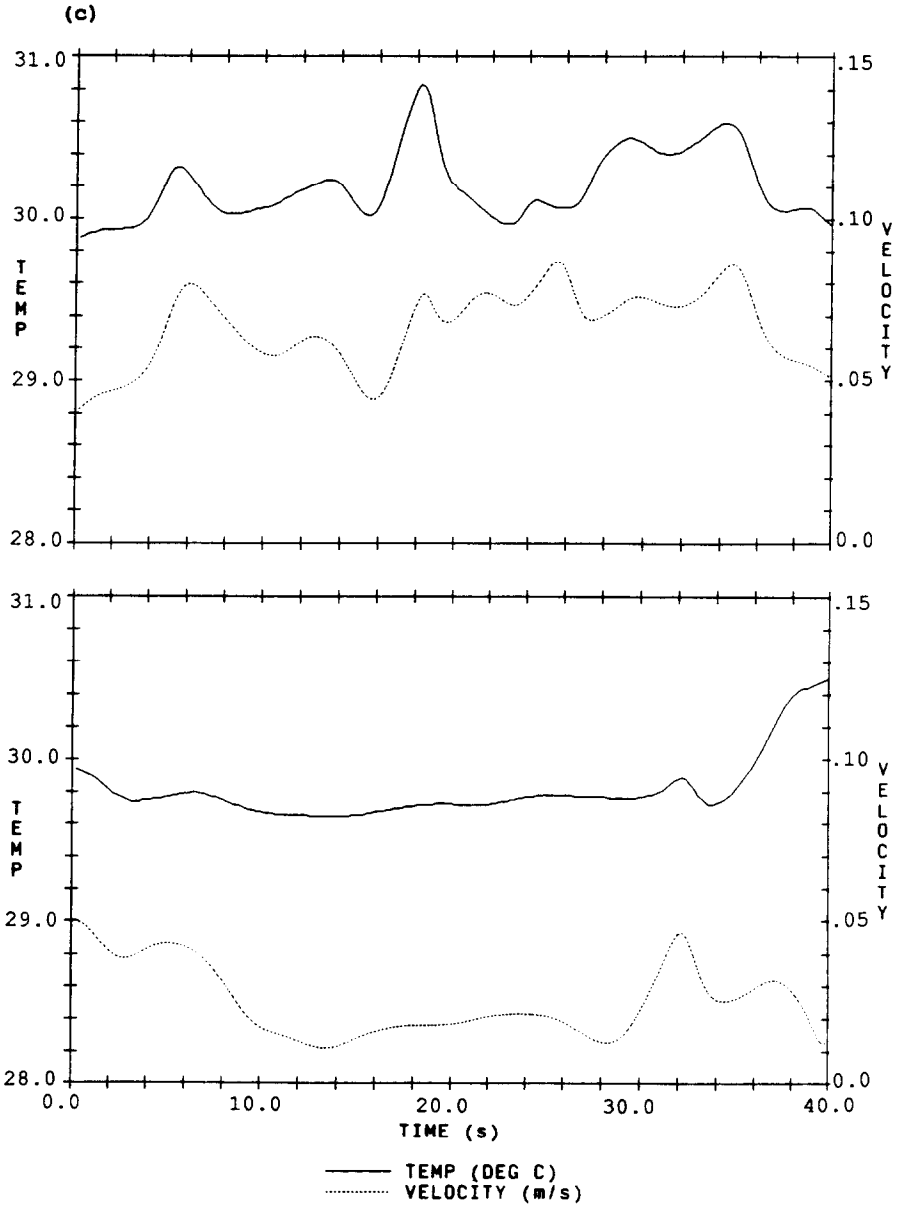

FIG. 5.—*Continued.*

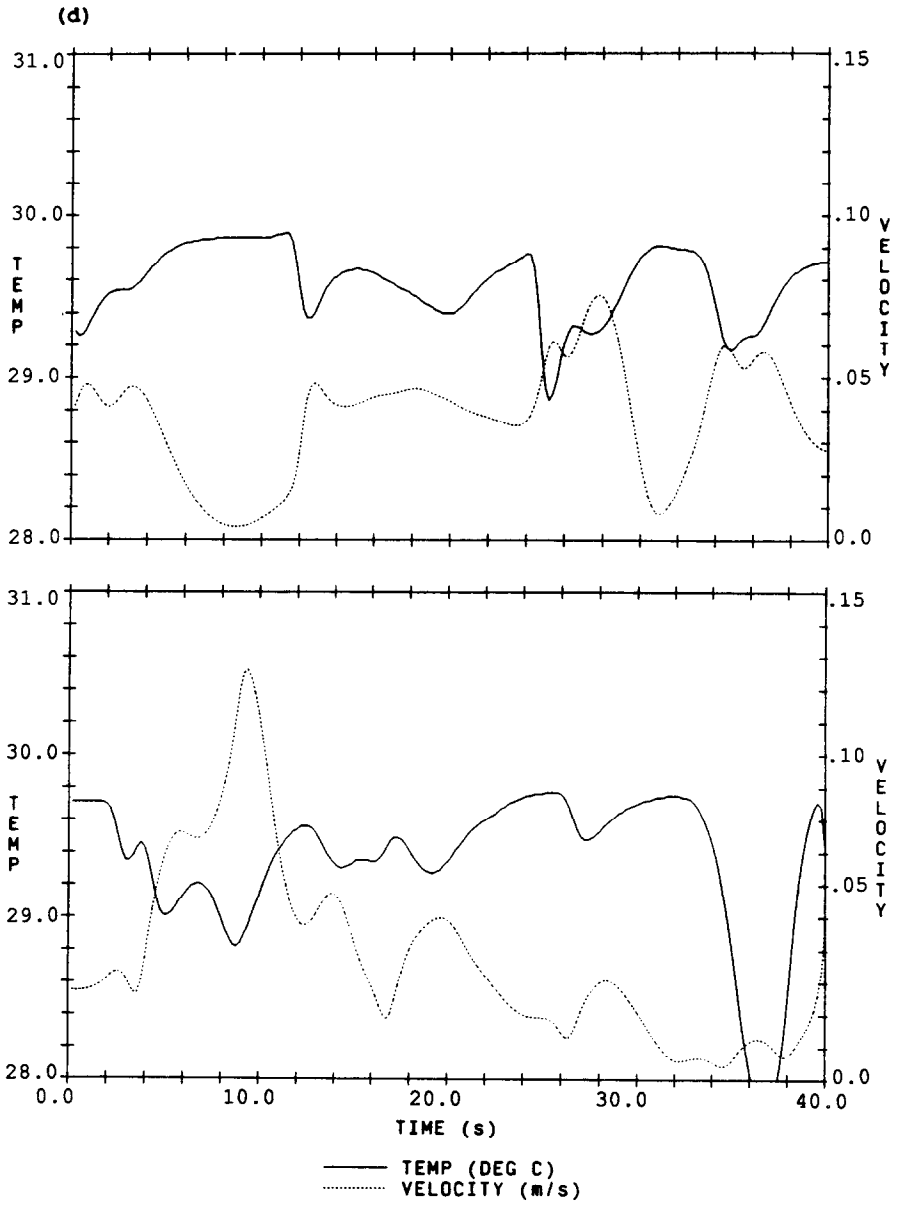

FIG. 5.—*Continued.*

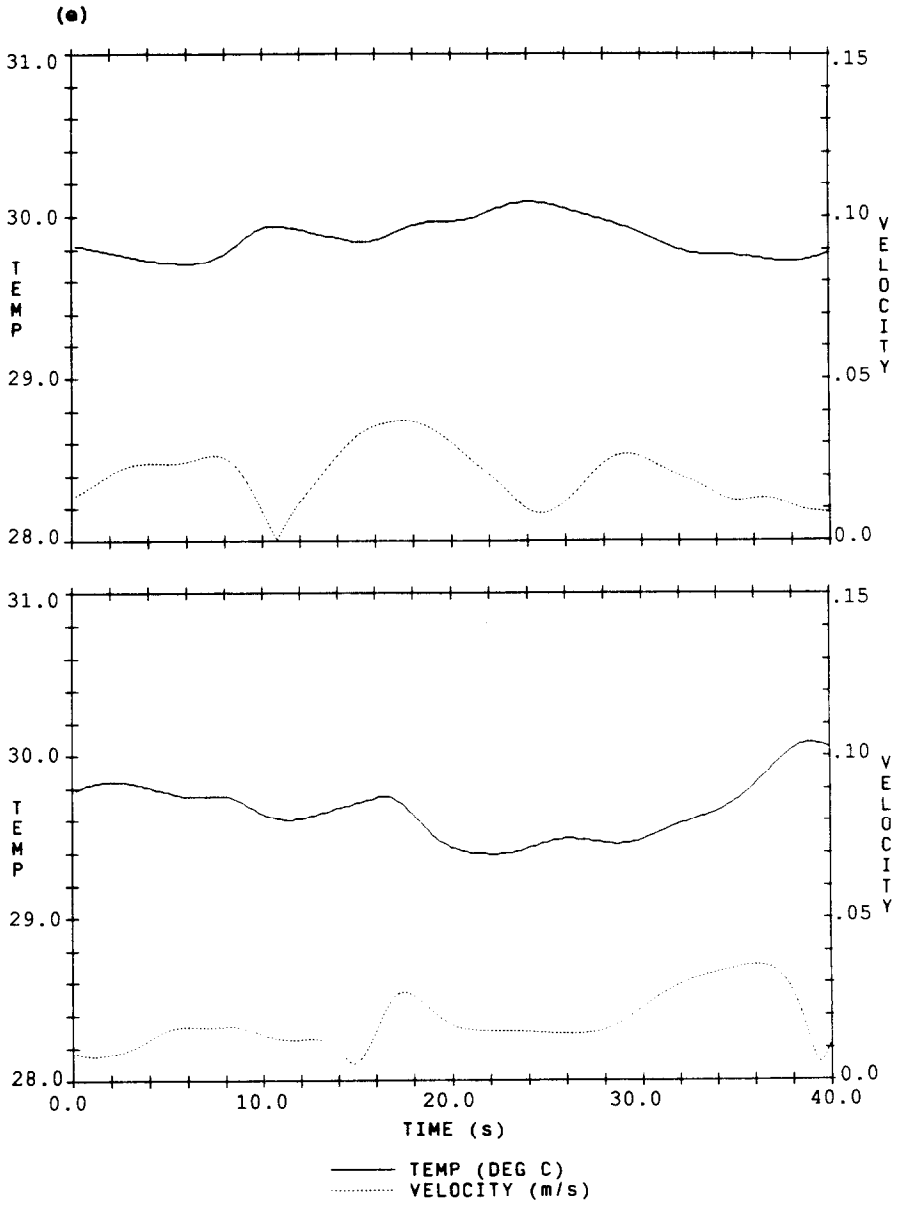

FIG. 5.—*Continued.*

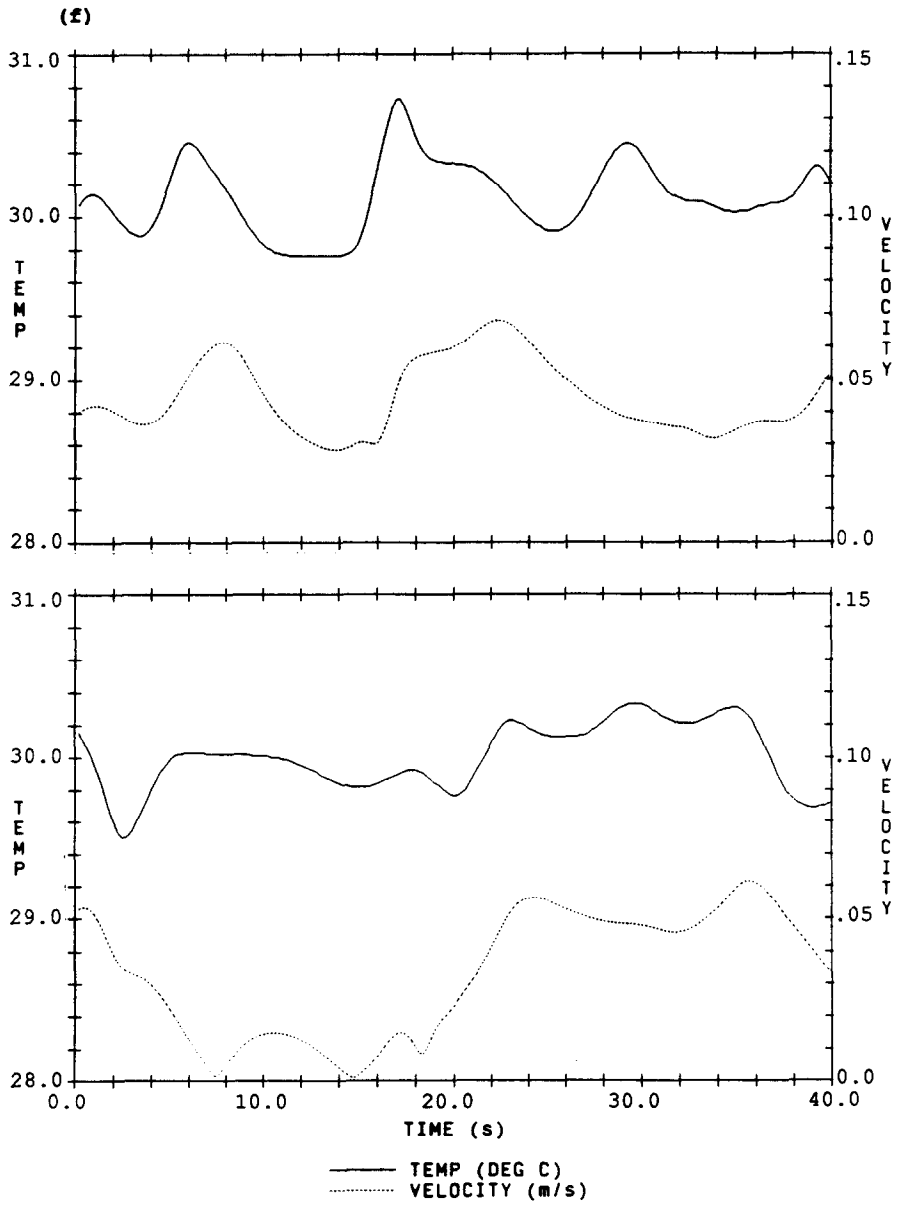

FIG. 5.—*Continued.*

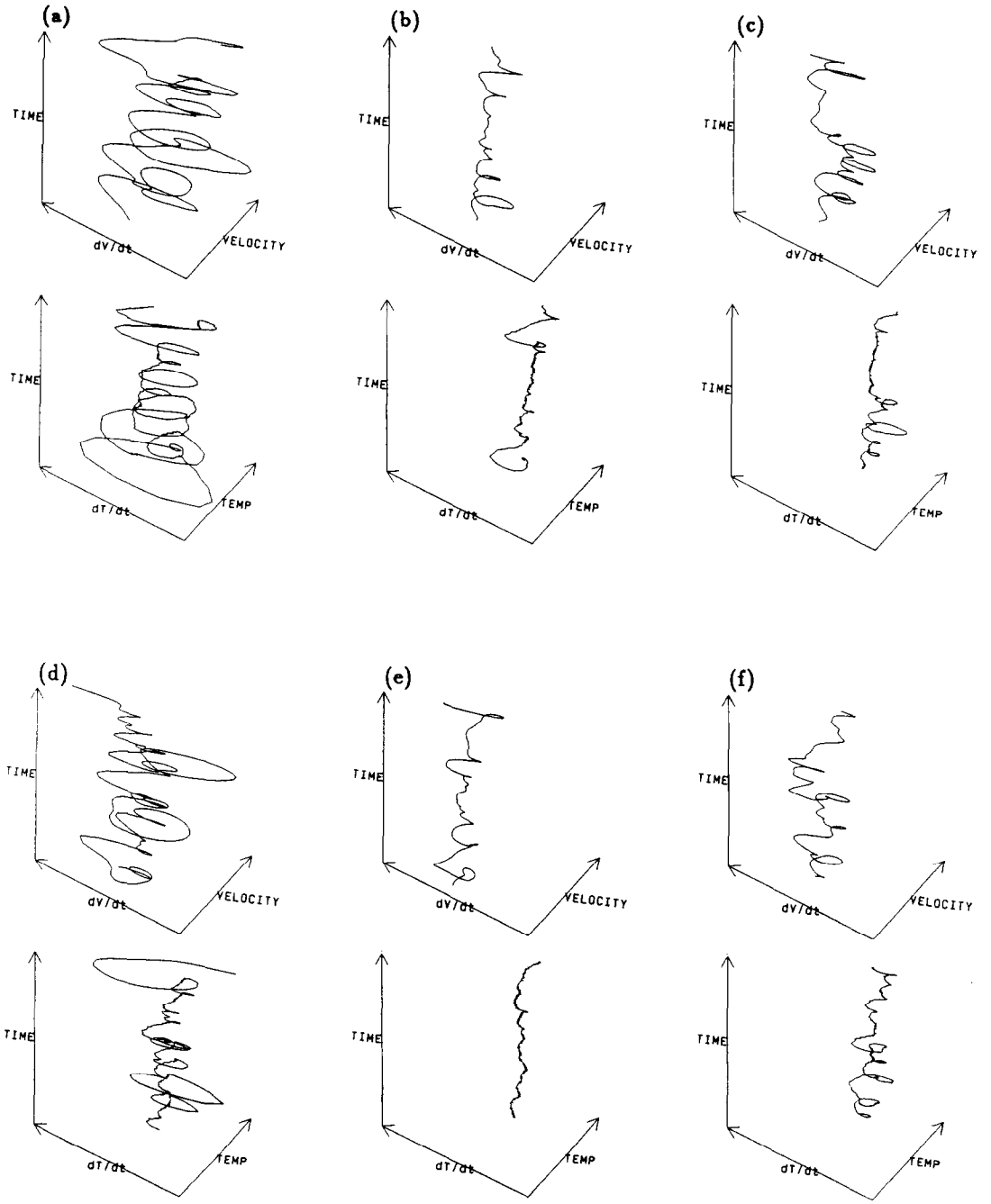

FIG. 6. Two-dimensional numerical phase-space plots of velocity and temperature. (a) (0.50L, 0.31H). (b) (0.70L, 0.31H). (c) (0.90L, 0.11H). (d) (0.50L, 0.82H). (e) (0.70L, 0.62H). (f) (0.90L, 0.72H).

temperature and velocity behave in an oscillatory nature with some incommensurable harmonics at the six chamber locations investigated as shown in Fig. 5. The magnitude and frequency of the oscillations were shown to be dependent upon the chamber location and the proximity of that chamber location to a Bénard cell. The greatest oscillatory behavior occurred at the chamber centerline between the upper baffles, with the core flow developing and subsequently dissipating as a result of the Bénard cell formation above the upper baffles and heat sources. Temperature and velocity tended to be inversely proportional, as would be expected in flow structures driven by buoyant forces with a fluid Prandtl number approaching one for which the rate that the velocity profile develops is equivalent to the rate that the thermal profile develops (Figs. 5(a), (b), and (d)). However, Figs. 5(c), (e), and (f) did not show this behavior, possibly due to the proximity of the chamber location to the movement of the low velocity core of a Bénard cell.

Phase-space or attractor plots of temperature and velocity, shown in Fig. 6, exhibited unique shapes at the six chamber locations resulting from a combination of steady state behavior which is represented by a fixed point in the phase-space, periodic behavior which is represented by a limit cycle in the phase-space and aperiodic behavior which is represented by a torus in the phase-space of temperature and velocity.

The experimental results demonstrated the transition of the flow structure through specific bifurcations, with the heat source temperature being the driving parameter for these transitions to occur. Figure 7 illustrates this behavior at chamber location ($0.70L$, $0.31H$). With an increasing heat source temperature, the velocity was shown to pass through transitions from steady state, periodic, aperiodic, and finally chaotic or random oscillatory behavior with high frequency incommensurable harmonics. Figure 8 compares the experimentally obtained temperature and velocity harmonics at the six chamber locations to the velocity harmonics obtained from the two dimensional numerical results. The oscillatory behavior of temperature was significantly attenuated due to the frequency response of the thermocouples and was therefore difficult to resolve and compare with velocity. However, the velocity behavior demonstrated unique differences in harmonics between the six chamber locations.

Experimental results showed chamber location ($0.70L$, $0.62H$), Fig. 8(e), to have the greatest variation in velocity while chamber location ($0.50L$, $0.82H$), Fig. 8(d), had the least. This is opposite to the numerical results which showed the greatest variation in velocity to be at chamber locations ($0.50L$, $0.31H$) and ($0.50L$, $0.82H$) and the least variation in velocity at chamber location ($0.70L$, $0.62H$). Experimental results, however, did show that chamber location ($0.50L$, $0.31H$), Fig. 8(a), had the greatest variation in velocity second to chamber location ($0.70L$, $0.62H$), Fig. 8(e), agreeing with the numerical results as to being one of the two chamber locations with the greatest velocity variations.

The experimental results showed unique transient behavior at each of the six chamber locations. Transition of velocity through a series of bifurcations showed a unique behavior in both amplitude and harmonics up to and including the steady oscillatory behavior. Experimental results also indicated a marginally stable flow structure that appeared to be easily perturbed by heat source temperature. Comparison of the numerically obtained velocity results to the experimentally obtained velocity data show good agreement in harmonic behavior for chamber locations ($0.50L$, $0.31H$), ($0.90L$, $0.11H$) and ($0.90L$, $0.72H$) in Figs. 5(a), (c) and (f), respectively. The numerical results appeared to have less high frequency harmonics than the experimental results, due in part to possible numerical damping. Comparison of the numerical and experimental results for chamber locations ($0.50L$, $0.82H$), ($0.70L$, $0.31H$) and ($0.70L$, $0.62H$) in Figs. 5(d), (b) and (e), respectively, showed poor agreement in the harmonic behavior of velocity.

Verification of the high velocity boundary layer region was performed by traversing the hot wire anemometer probe toward the vertical end wall. The location of this high velocity region was determined when there was an observable increase in the indicated

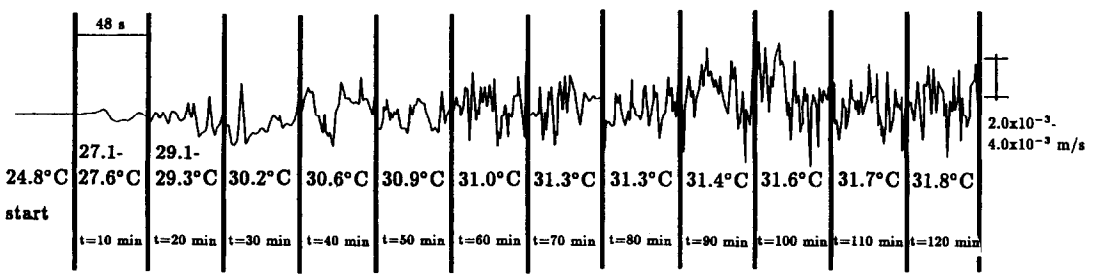

FIG. 7. Time-dependent experimental results for velocity at chamber location ($0.70L$, $0.31H$) with increasing heat source temperature.

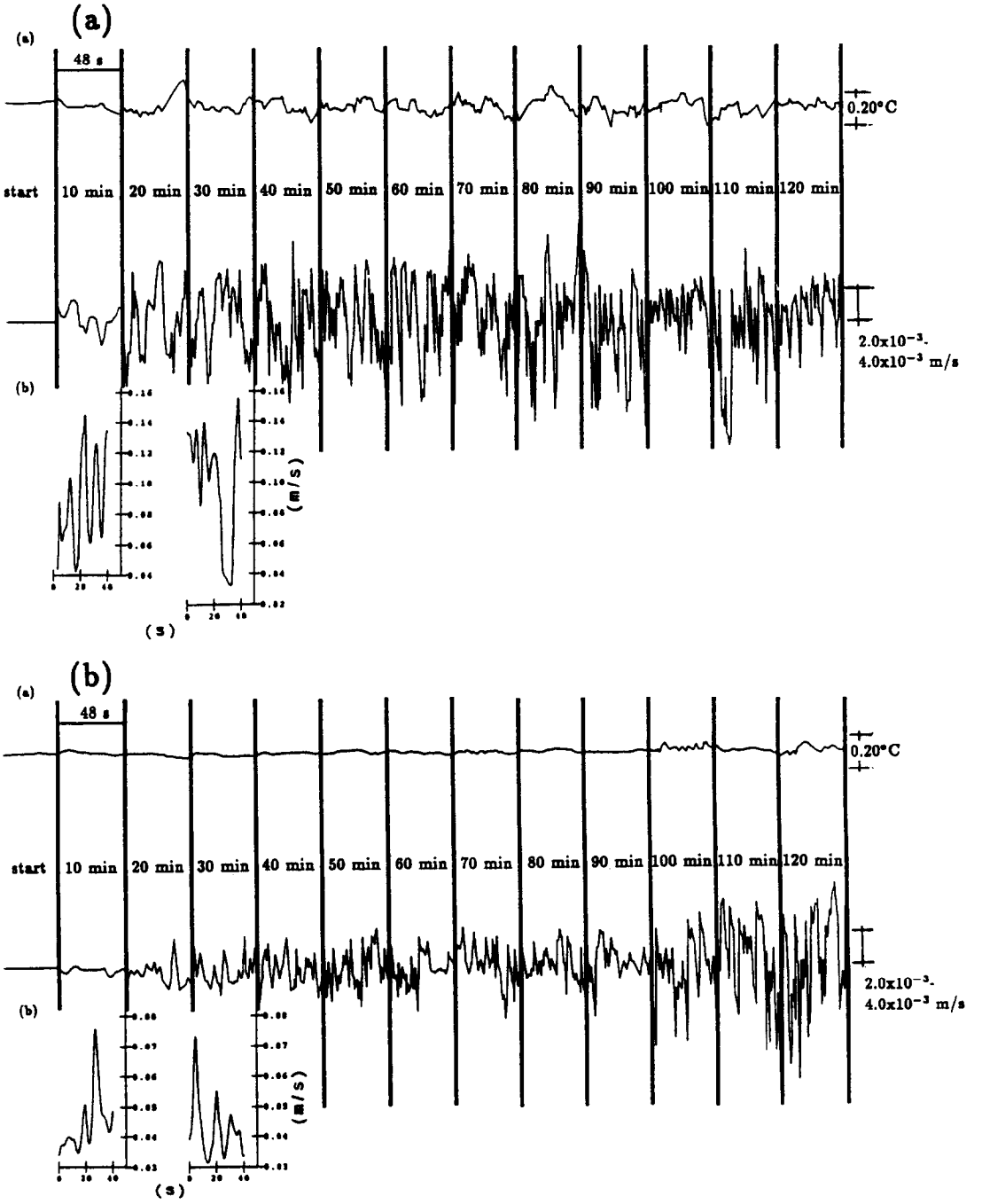

FIG. 8. Comparison of: (a) time-dependent experimental results for velocity and temperature and (b) time-dependent numerical results for velocity at chamber locations: (a) $(0.50L, 0.31H)$; (b) $(0.70L, 0.31H)$; (c) $(0.90L, 0.11H)$; (d) $(0.50L, 0.82H)$; (e) $(0.70L, 0.62H)$; (f) $(0.90L, 0.72H)$.

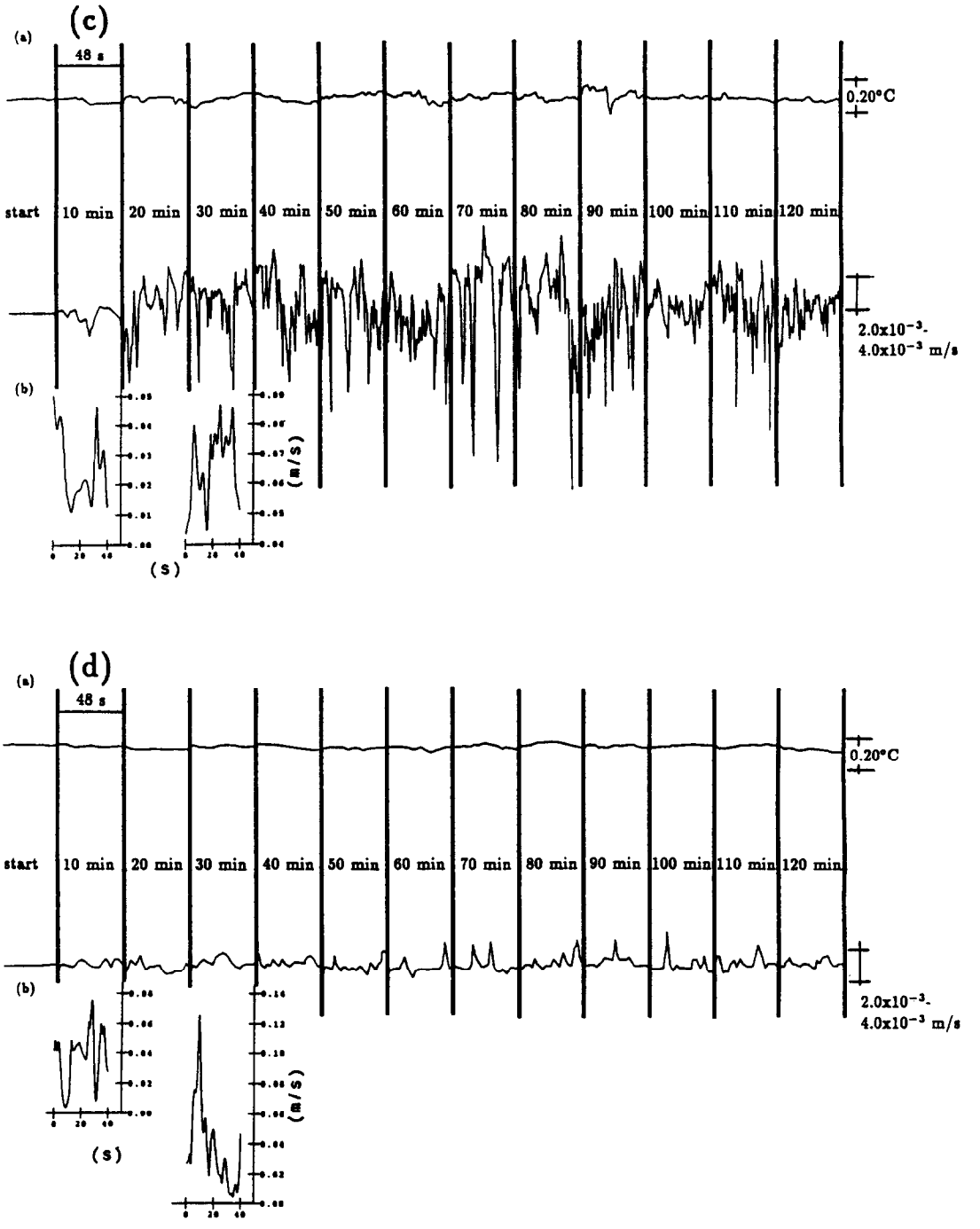

FIG. 8.—*Continued.*

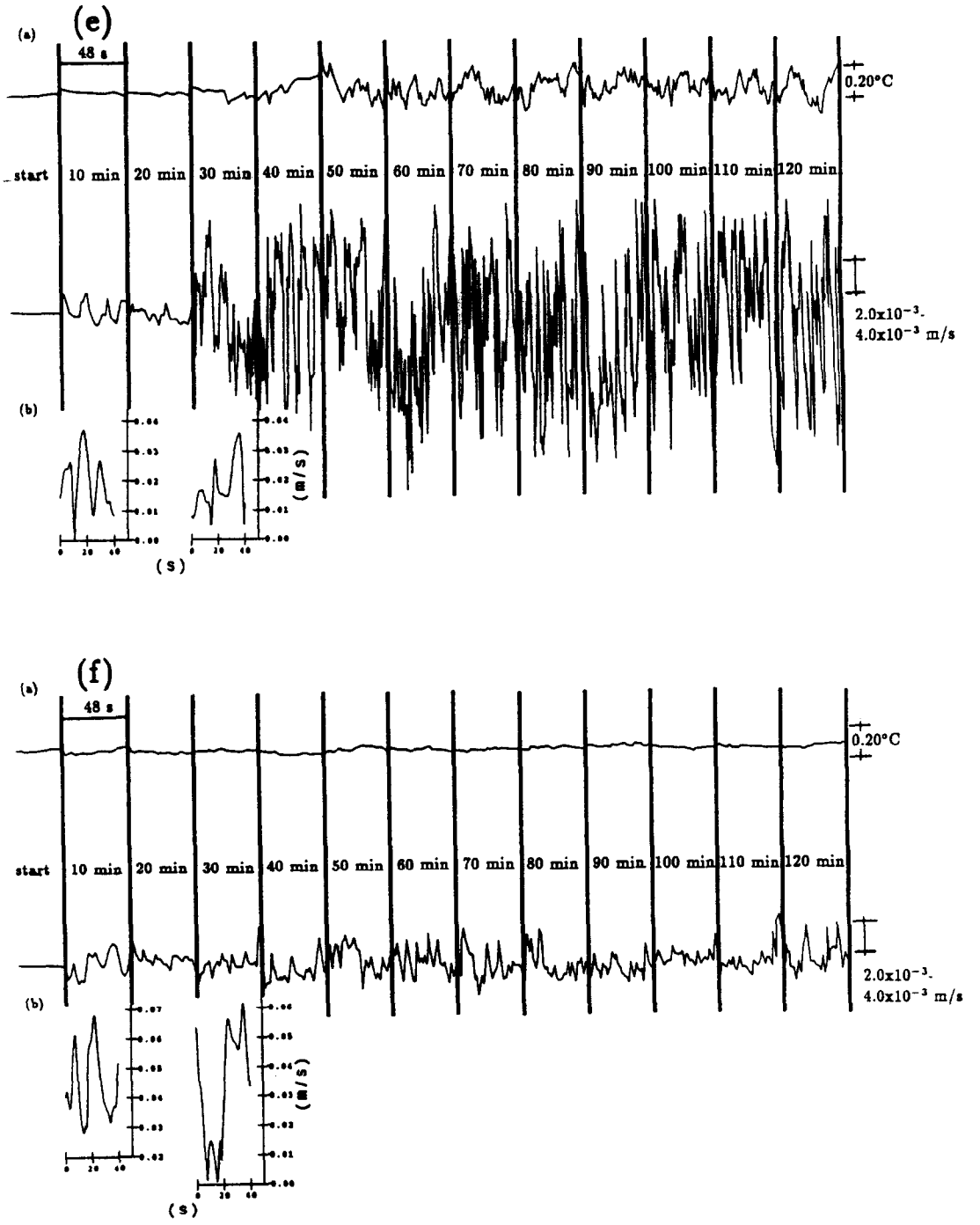

FIG. 8.—*Continued.*

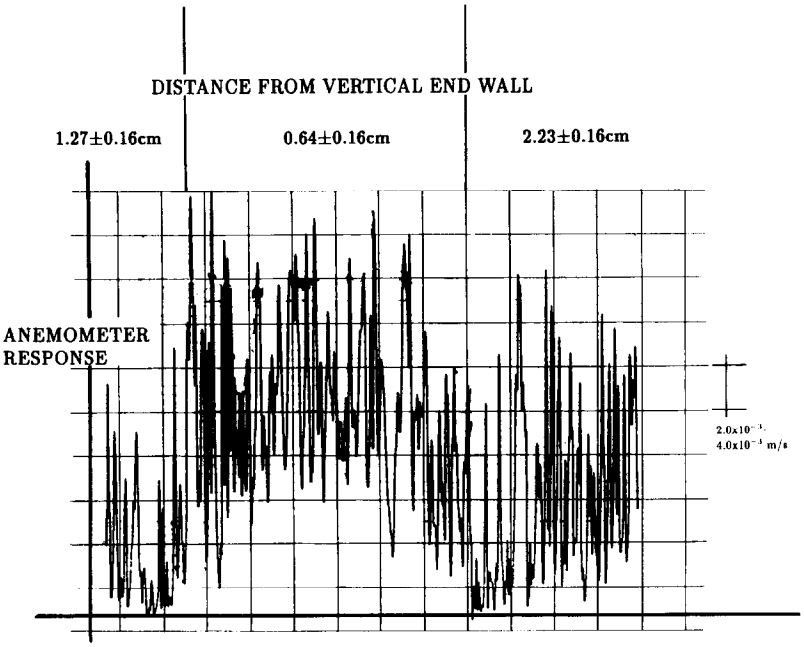

FIG. 9. Experimental results for locating the high velocity boundary layer region at $0.67H$.

velocity from that of a baseline velocity outside the confines of the high velocity region. Figure 9 shows the results of these measurements, confirming the presence of a high velocity region between the vertical end wall and 0.64 ± 0.16 to 1.27 ± 0.16 cm with a vertical location of $0.67H$.

It was found that the numerical and experimental techniques were each limited when describing the time-dependent characteristics of a random and marginally stable flow structure. A trade-off had to be reached when choosing the numerical grid size and time step increment so that most of the frequency harmonics could be captured, while minimizing the computational time. The experimental measurement of the low velocities present in the chamber resulted in sensor-induced inaccuracies. The measurements of the small temperature differences were significantly attenuated by the thermocouple frequency response. However, the numerical and experimental results obtained demonstrate similar harmonics and time-dependent behavior of the developing flow structure.

CONCLUSIONS

The flow structure within large baffled chambers with internal heat sources has been investigated. Unique harmonics and time-dependent behavior due to mixed convection were seen in both the numerical solution and the laboratory experimental model. Transition from a stable, steady state flow structure to one that is periodic in time, aperiodic, and finally chaotic are examples of specific bifurcations which were found with variations in Rayleigh number, Prandtl number, and altered geometry. The numerical solution and experimental measurements of the harmonics of the velocity and temperature showed similar frequency behaviors.

Acknowledgements—This research was conducted at Wright State University, Dayton, Ohio. Partial support was provided by the Wright Research and Development Center located at Wright-Patterson AFB, Ohio.

REFERENCES

1. S. M. Bajorek and J. R. Lloyd, Experimental investigation of natural convection in partitioned enclosures, *ASME J. Heat Transfer* **104,** 527–532 (1982).
2. N. C. Markatos and M. R. Malin, Mathematical modelling of buoyancy-induced smoke flow in enclosures, *Int. J. Heat Mass Transfer* **25,** 63–75 (1982).
3. R. E. Powe and R. O. Warrington, Jr., Natural convection heat transfer between bodies and their spherical enclosure, *ASME J. Heat Transfer* **105,** 440–446 (1983).
4. M. W. Nansteel and R. Grief, Natural convection in undivided and partially divided rectangular enclosures, *ASME J. Heat Transfer* **103,** 623–629 (1981).
5. E. M. Sparrow, P. C. Stryker and M. A. Ansari, Natural convection in enclosures with off-center innerbodies, *Int. J. Heat Mass Transfer* **27,** 49–56 (1984).
6. R. O. Warrington, Jr. and R. E. Powe, The transfer of heat by natural convection between bodies and their enclosures, *Int. J. Heat Mass Transfer* **28,** 319–330 (1985).
7. M. November and M. W. Nansteel, Natural convection in rectangular enclosures heated from below and cooled along one side, *Int. J. Heat Mass Transfer* **30,** 2433–2440 (1987).
8. J.-H. Lee and R. J. Goldstein, An experimental study of natural convection heat transfer in an inclined square enclosure containing internal energy sources, *ASME J. Heat Transfer* **110,** 345–349 (1988).
9. S. Ostrach and W. J. Austin, Natural convection in

enclosures, *ASME J. Heat Transfer* **110,** 1175–1190 (1988).
10. K. T. Yang, Transitions and bifurcations in laminar buoyant flows in confined enclosures, *ASME J. Heat Transfer* **110,** 1191–1204 (1988).
11. R. L. Carpenter and R. L. Beethe, Cones, cone angles, plenums, and manifolds, *Proc. Workshop Inhalation Chamber Tech.* (Edited by R. T. Drew), Brookhaven National Laboratory Report BNL 51318 UC-48 (1981).
12. R. O. Moss, A chamber producing uniform concentrations of particulates for exposure of animals on tiers separated by catch pans, *Proc. Workshop Inhalation Chamber Tech.* (Edited by R. T. Drew), Brookhaven National Laboratory Report BNL 51318 UC-48 (1981).
13. D. R. Hemenway, R. L. Carpenter and O. R. Moss, Inhalation toxicology chamber performance: a quantitative model, *Am. Ind. Hygiene Assoc. J.* **43,** 120–127 (1982).
14. R. L. Beethe, R. K. Wolff, L. C. Griffis, C. H. Hobbs and R. O. McClellan, Evaluation of a recently designed multi-tiered exposure chamber, Department of Energy Contract No. EY-76-C-04-11013 (1979).
15. O. R. Moss, J. R. Decker and W. C. Cannon, Aerosol mixing in an animal exposure chamber having three levels of caging with excreta pans, *Am. Ind. Hygiene Assoc. J.* **43,** 244–249 (1982).
16. H. C. Yeh, G. J. Newton, E. B. Barr, R. L. Carpenter and C. H. Hobbs, Studies of the temporal and spatial distribution of aerosols in multi-tiered inhalation exposure chambers, *Am. Ind. Hygiene Assoc. J.* **47,** 540–545 (1986).
17. K. L. Yerkes and A. Faghri, An experimental and numerical simulation mixed convection in large baffled rectangular chambers, *Int. J. Heat Mass Transfer* **34,** 1525–1542 (1991).
18. J. L. Mauderly, Respiration of F344 rats in nose-only inhalation exposure tubes, *J. Appl. Toxicol.* **6,** 25–30 (1986).
19. D. B. Spalding, Mathematical modeling of fluid-mechanics, heat transfer and chemical reaction processes, a lecture course, CFDU Report, HTS/80/1, Imperial College, London (1980).
20. S. V. Patankar, *Numerical Heat Transfer and Fluid Flow*, pp. 102–104. Hemisphere, New York (1980).
21. TSI Technical Bulletin, Measurements in Low Velocity Gases, TB 14.

ANALYSE DE LA CONVECTION MIXTE DANS DES GRANDES CHAMBRES RECTANGULAIRES AVEC PARTITION ET SOURCES DE CHALEUR INTERNES

Résumé—On essaie de déterminer les effets de la convection mixte sur la structure de l'écoulement dans des grandes chambres avec partition et sources de chaleur internes. Les baffles et les sources de chaleur sont placés symétriquement par rapport à l'axe vertical et on maintient constantes et uniformes une vitesse d'entrée, une température d'entrée et de paroi. Les résultats expérimentaux dépendant du temps et ceux numériques bidimensionnels sont comparés à différentes positions dans la chambre pour montrer la transition de la structure de l'écoulement à travers une séquence de bifurcations avec accroissement des températures de source interne.

UNTERSUCHUNG DER MISCHKONVEKTION IN GROSSEN UNTERTEILTEN RECHTECKKAMMERN MIT INNEREN WÄRMEQUELLEN

Zusammenfassung—Es wird über den Abschluß einer Untersuchung zur Bestimmung des Einflusses der Mischkonvektion auf die Strömungsstruktur in großen unterteilten Rechteckkammern mit inneren Wärmequellen berichtet. Die Unterteilungen und die inneren Wärmequellen sind symmetrisch entlang der senkrechten Achse angeordnet, während die Eintrittsgeschwindigkeit, die Eintrittstemperatur sowie die Wandtemperatur konstant und gleichförmig sind. Der zeitliche Verlauf der gemessenen und der zweidimensional berechneten Ergebnisse wird für die unterschiedlichen Kammern verglichen. Dadurch kann der Übergang der Strömungsstruktur durch eine Reihe von Aufspaltungen bei steigender Temperatur der inneren Wärmequellen gezeigt werden.

АНАЛИЗ СМЕШАННОЙ КОНВЕКЦИИ В КРУПНЫХ ПЕРЕГОРОЖЕННЫХ КАМЕРАХ ПРЯМОУГОЛЬНОГО СЕЧЕНИЯ С ВНУТРЕННИМИ ИСТОЧНИКАМИ ТЕПЛА

Аннотация—Исследуется влияние смешанной конвекции на структуру течения в крупных перегороженных камерах с внутренними источниками тепла. Перегородки и внутренние источники тепла размещались симметрично относительно вертикальной оси, причем поддерживались постоянные и однородные скорость и температура на входе, а также температура стенки. Сравнение нестационарных экспериментальных и двумерных численных результатов при различных расположениях камеры показывает, что структура течения претерпевает ряд бифуркаций по мере возрастания температуры внутренних источников тепла.